Jalón, E., Hoang, T., Rubio-López, A., & Santiuste, C. (2018). Analysis of low-velocity impact on flax/PLA composites using a strain rate sensitive model. Composite Structures, 202, 511-517.

doi:https://doi.org/10.1016/j.compstruct.2018.02.080

Analysis of low-velocity impact on flax/PLA composites using a strain rate sensitive model

E. Jalón[a]

T. Hoang[a]

A. Rubio-López[b]

C. Santiuste[a, *]

csantius@ing.uc3m.es

[a]Department of Continuum Mechanics and Structural Analysis, Universidad Carlos III de Madrid, Avda de la Universidad 30, 28911 Leganés, Spain

[b]INDRA TGP, Ctra. Loeches, 9, 28850 Torrejón de Ardoz, Spain

*Corresponding author.

Abstract

The mechanical behaviour of conventional composites is usually assumed as linear-elastic up to failure. However, the mechanical behaviour of natural fibres based composites is non-linear with a significant influence of strain-rate. This study presents a FEM model to analyse the impact behaviour of flax/PLA composites. The constitutive model includes the consideration of plastic strains and the influence of strain rate. The model was validated through comparison with low-velocity impact tests. Numerical prediction were in agreement with experimental results conducted with two impactor nose at different impact energies.

Keywords: Biocomposite; Impact behaviour; Finite element analysis (FEA); Natural fibres

1 Introduction

During the last years, natural fibres have been introduced as reinforcements in order to develop biodegradable composites [1,2]. In terms of matrices, non-biodegradable polymeric materials (such as epoxy, polyethylene or polypropylene) are typically used with natural fibres [3]. However, biodegradable matrices (such as polysaccharides, proteins, polyesters, lignin, lipids, etc.) can also be used to obtain 100% eco-sustainable composites [3–5]. The introduction of fully biodegradable composites can reduce the use of non-biodegradable materials and non-renewable resources. The main advantages of biocomposites are their low cost, lightweight and less energy consumption for their production. Biodegradable composites are applied in different industrial applications and engineering fields such as packaging, biotechnology, automotive industry or environmental technology, offering significant advantages in terms of environmental impact, cost and weight [3,6–8].

One of the most relevant drawbacks of traditional composites is their sensitivity under low-velocity impacts [9]. Therefore, there are numerous studies about the low-velocity impact behaviour of traditional composites. The development of predictive FEM models has been used to get a better understanding of the impact behaviour of composites [10–13]. For instance, Antonucci et al. [10] used cohesive elements to predict delamination evolution on carbon fibres composites under multiple low-velocity impact tests. Ivañez et al. [11] studied the low-velocity impact behaviour of sandwich beams. The FEM model results were used to explain the influence of foam core on induced damage during impact. The behaviour of traditional composites reinforced with carbon or glass fibres can be usually assumed as linear elastic up to failure, thus the development of predictive FEM models has been focused on the implementation of accurate failure criteria and the prediction of damage evolution [12,13].

However, very few studies analysed the behaviour of biodegradable composites under low-velocity impacts, being most of them experimental [14–16]. Huber et al. [14] studied the behaviour of all-cellulose composites (ACCs) made from Cordenka fibres under low-velocity impact produced by a drop weight test, they found that ACC laminates exceed the impact properties of most conventional composites. Dhakal and his co-workers [15] investigated the fibre weave architecture effect on the low-velocity impact response of jute fibre reinforced methacrylated soybean oil composite, founding that woven laminates possess better toughness properties. Rubio-López et al. [16] compared the compression after impact properties of carbon and flax reinforced composites. The normalised compression after impact strength was higher in flax composites than in carbon composites.

The promising results of these few studies means that biodegradable composites can be competitive in terms of strength under low-velocity impacts. However, the development of numerical models to predict the impact

behaviour of biodegradable composites is an almost unexplored field. The first numerical model was presented by Rubio-López et al. [17] to predict the low velocity behaviour of ACC composite plates using a FEM model. This model was based on the traditional composites hypotheses: linear-elastic behaviour up to failure and strain rate independent behaviour [11,13].

There are some alternatives to model the failure of composites reinforced with natural fibres [18–21]. Wang et al. [18] proposed a multiscale approach based upon the micromechanical analysis of multiple damage events to predict the behaviour of unidirectional composites subjected to tensile loading. Pan et al. [19] developed a micromechanical model to analyse the influence of moisture absorption on the mechanical properties of natural fibre based composites. Also shear-lags models have been proposed to predict the non-linear behaviour of biocomposites [20,21]. However, these constitutive models have not been implemented in a FEM model to analyse the impact behaviour of biocomposites.

On the other hand, different studies have proved the strong influence of the strain-rate on the behaviour of biocomposites and their non-linear behaviour [22,23]. Therefore, traditional composite models assuming linear-elastic behaviour up-to-failure can be implemented in biocomposites only as a first approach.

This paper presents a FEM model for biodegradable composites considering viscoplastic behaviour. The non-linear mechanical behaviour of biocomposites is defined as a function of strain-rate and a failure criterion based on maximum strains is included to delete damaged elements. FEM model was implemented in ABAQUS/Explicit software. The results are validated through the comparison with experimental tests conducted on a drop-weight tower with different impactor noses and different impact energies. Biodegradable composite plates were manufactured from flax woven fibres and poly-lactic acid (PLA) matrix.

2 Experimental set-up

Flax woven fibres were combined with PLA matrix to manufacture the specimens. PLA 10361D was acquired from Natureworks LLC, and it is defined as a biodegradable thermoplastic resin specifically aimed as a natural fibre binder. Biocomposites were manufactures by compression moulding process. First, five PLA layers and four woven fibres plies were alternatively stacked, then the laminate was place between two thermoheated plates, and pressure was applied by a universal testing machine. An optimization of the manufacturing process was performed as reported in Ref. [24], revealing that the optimum manufacturing parameters are obtained with plates at 185 °C, applying 16 MPa of pressure during 3 min after 2 min of preheating applying 2 MPa. The fibre weight ratio was stated in 65% as recommended by Ochi et al. [25]. A resulting woven laminate of four layers with a thickness of 2.64 ± 0.11 mm was obtained. The specimens were cut into square plates of 80×80 mm.

Woven fibres and PLA plies were maintained in an oven under 95 °C during 4 h before the compression moulding process to remove water content. All the materials were stored in stable constant conditions of 46% RH and 20 °C before and after the manufacturing process to control the environmental conditions influence.

A CEAST Fractovis 6875 drop weight tower was used to carry out the low-velocity impact tests. The specimens were clamped with a free circular area of 55 mm diameter. The drop-weight tests were carried out by using an impactor with hemispherical noses of 12.7 mm and 20 mm. The impactor weights were 3.76 kg and 3.815 kg. Impact energy was modified from 3.8 J to 10 J to verify the model capacity to reproduce different damage sizes. The maximum value of impact energy was below the penetration energy, so that all the specimens were damaged but not penetrated. This range of impact energies was selected to produce a barely visible damage, this is a critical problem in traditional composite because it can lead to a significant reduction in residual strength.

3 Model description

3.1 Constitutive model

According to the stress-strain curves shown in Fig. 1, there is a significant influence of strain-rate on the mechanical behaviour of biocomposites. Details about the characterization tests can be found in a previous work [22]. Fig. 1 shows that mechanical behaviour is clearly non-linear, stiffness and strength increase with strain rate, while ultimate strain decreases. Stress-strain curves can be directly introduced in ABAQUS/Explicit to include the influence of strain-rate in a FEM model. However, the strain-rates of the characterization tests ranged from $2.08 \cdot 10^{-4}$ to $8.33 \cdot 10^{-3}\,s^{-1}$, and the expected strain-rates during impact are much higher, thus a constitutive model is necessary to predict the mechanical behaviour at higher strain rates.

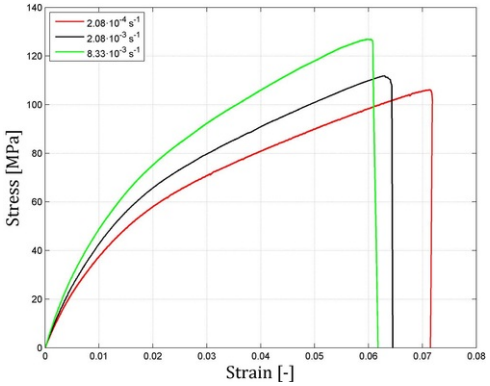

Fig. 1 Stress-strain curves obtained experimentally under different strain rates: $2.08 \cdot 10^{-4}\,s^{-1}$, $2.08 \cdot 10^{-3}\,s^{-1}$ and $8.33 \cdot 10^{-3}\,s^{-1}$.

A constitutive model presented in a previous work [22] was used to properly define the yield stress and to obtain the mechanical behaviour under high strain-rates. This constitutive model is based on a rheological approach including three branches as shown in Fig. 2.

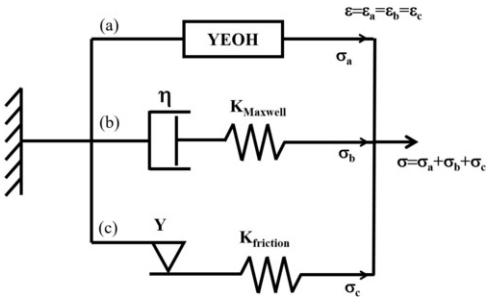

Fig. 2 Rheological model scheme. (a) non-linear elastic branch, (b) viscoelastic branch, (c) plastic branch.

Branch (a) describes non-linear elasticity through a Yeoh model [26], this model is based on incompressible materials, and thus, the energy density function depends on the first invariant of the left Cauchy-Green deformation tensor. The constitutive equation for Yeoh model under uniaxial extension is defined in Eq. (1):

$$\sigma_{Yeoh} = \frac{2\epsilon(3+\epsilon(3+\epsilon))((1+\epsilon)^2 C_1 + \epsilon^2(3+\epsilon)(2(1+\epsilon)C_2 + 3\epsilon^2(3+\epsilon)C_3)}{(1+\epsilon)^2} \quad \textbf{(1)}$$

where C_1,C_2 and C_3 are three elastic constants.

Branch (b) considers viscous effects defined through a Maxwell model. Maxwell element is given by a spring and a dashpot in series, the stress is the same in both elements and the total strain is the sum of the spring and dashpot strains. Thus, mechanical response of Maxwell element is described by Eq. (2):

$$\dot{\sigma}_{Maxwell} + \frac{K}{\eta} \cdot \sigma_{Maxwell} = K \cdot \dot{\epsilon} \quad \textbf{(2)}$$

where ?? is the dashpot constant, K is the spring constant and $\dot{\epsilon} = \dot{\epsilon}_{dashpot} + \dot{\epsilon}_{spring}$.

Branch (c) introduced the plasticity by a frictional analogy to the Maxwell model, the model includes a spring and frictional element in series. The model stiffness is dominated by the spring element until the frictional element is activated, the role of the frictional element is to stablish a limit for the stress equal to Y. The definition of the stress-strain relationship is defined by Eq. (3):

$$\begin{aligned} &if\ \varepsilon < \varepsilon_y \rightarrow \sigma_{Friction} = K_{friction} \cdot \epsilon \\ &if\ \varepsilon \geqslant \varepsilon_y \rightarrow \sigma_{Friction} = Y \end{aligned} \quad \textbf{(3)}$$

The constitutive equation of the global model is given by sum of the three branches, Eq. (4):

$$\sigma = \sigma_{Yeoh} + \sigma_{Maxwell} + \sigma_{Friction} \quad \textbf{(4)}$$

More detail about the model can be found in Ref. [22] where the model was calibrated and validated for three different biocomposites reinforced with flax, cotton and jute fibres. The values of the material parameters are shown in Table 1.

Table 1 Parameters of the constitutive model for flax/PLA biocomposites [22].

$K_{Maxwell}$	1.08 GPa
$K_{friction}$	2.58 GPa
η	230 GPa·s
Y	12.3 MPa
C_1	338 MPa
C_2	−18.1 GPa
C_3	656 GPa

According to the constitutive model, yield stress was defined as a function of strain rate. For instance, yield stress was equal to 23 MPa for a strain rate of 2.08e−4 s^{-1} and equal to 47.1 MPa for a strain rate of 8.33e−3 s^{-1}.

Additionally, an erosion criterion was included in the FEM to delete damaged elements considering the influence of strain rate on the ultimate strain observed in experimental tests. A VUSDFLD user subroutine developed in ABAQUS/Explicit was used to define a maximum strain criterion. This criterion allows the removal of the elements that presents strains higher than the maximum defined as a function of strain rates.

Cohesive elements were not included to predict de-bonding between plies because delamination were not observed in experimental tests. Thus, perfect bonding between plies was considered.

3.2 Geometry and mesh

The geometry of the model reproduces the experimental drop-weight tests described in the previous section. The composite consisted on a circular plate of diameter (D_p) 55 mm and thickness (t_p) 2.55 mm. Two different impactors had been used to model the impactor bar. For simplicity, only the hemispherical nose of the impactors was modelled in the simulation. They were modelled as a hemispherical solid of two different diameters ($D_{s_{12.7\ mm}}$) 12.7 mm and ($D_{s_{20\ mm}}$) 20 mm with a mass of 3.7 and 3.815 kg, respectively, as shown in Fig. 3. The impactor was modelled using linear elastic behaviour (Young modulus E = 210 GPa, Poisson ratio μ = 0.3) since no permanent deformations after impact were found.

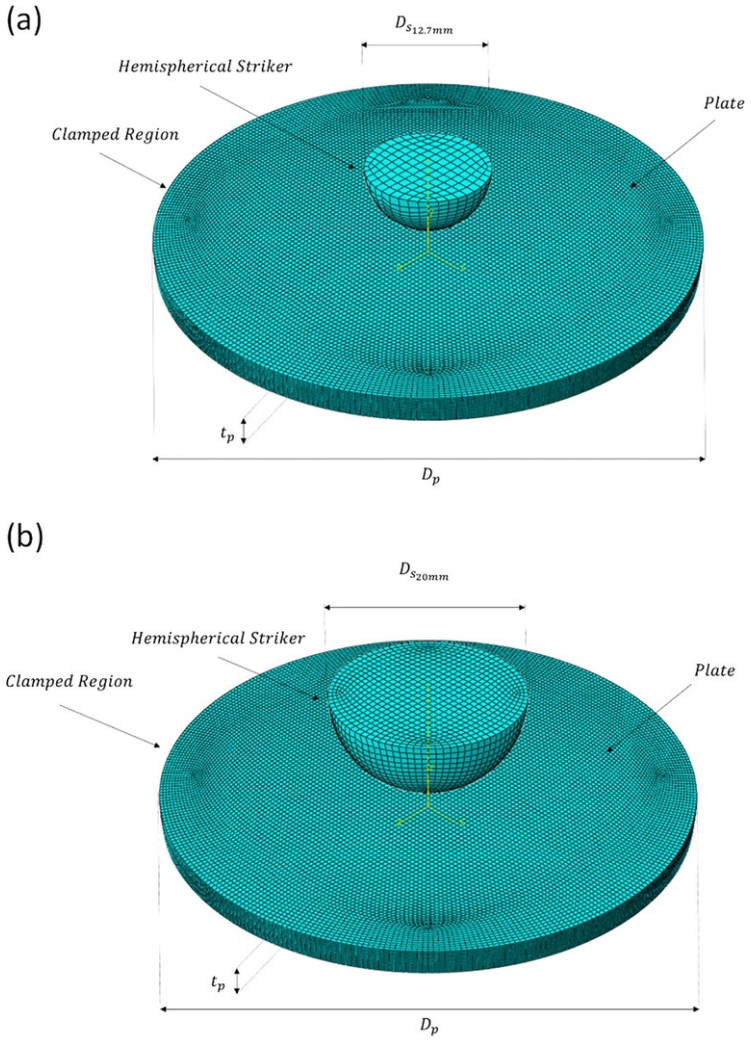

Fig. 3 Mesh and geometry of the FEM models. (a) Impactor nose with ϕ12.7 mm. (b) Impactor nose with ϕ20 mm.

The external surface of the plate was clamped in order to reproduce the experimental drop-weight tests boundary condition. Moreover, an interaction contact was defined between the impactor surface and the node region of the plate to consider the contact of the impactor surface with all the composite plies. The interaction was modelled using the algorithm surface-node surface contact available in ABAQUS/Explicit.

A mesh sensitivity study was conducted to analyse the influence of mesh size. The selected mesh for the plate had 172,860 linear brick elements, with reduced integration (C3D8R). The strikers were also modelled with 2340 and 9680 brick elements (C3D8R) for the impactors of 12 mm and 20 mm of diameter, respectively.

4 Results and discussion

Numerical results were validated through comparison with experimental data obtained in drop-weight tests. Fig. 4 shows the comparison between the experimental and numerical results in terms of contact force history with impactor nose of ϕ12.7 mm. There is a reasonable agreement between numerical and experimental curves. The evolution contact force was similar for all the impact energies. First, the impact force increased because of the contact between the impactor and the plate up to the damage onset. Then, there is a plateau while damage is progressing in the composite plate. Finally, contact force drops to zero when the impactor rebounded from the plate. The FEM

model was able to reproduce all the stages with a reasonable accuracy.

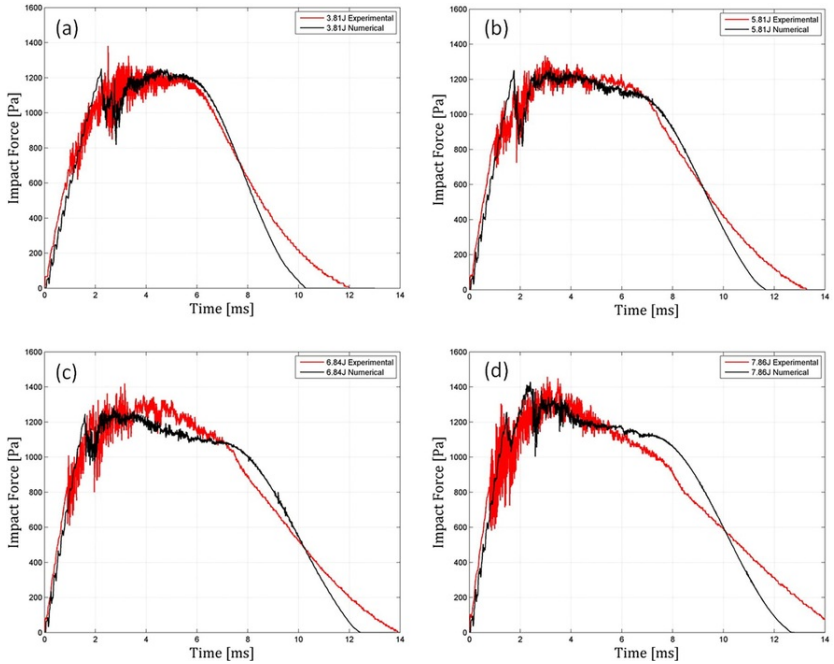

Fig. 4 Contact force history for different impact energies. Impactor nose with ϕ12.7 mm. (a) Eimp = 3.81 J. (b) Eimp = 5.81 J. (c) Eimp = 6.84 J. (d) Eimp = 7.86 J.

Fig. 5 shows that numerical predictions agreed with the experimental results in terms of absorbed energy evolution. The evolution of absorbed energy follows the well-known trend in low-velocity impacts. During the first stage, absorbed energy increases up to the value of impact energy. At this point, all the kinetic energy is absorbed by the composite plate and the impactor velocity is zero. Then, the absorbed energy decreases while impactor is bouncing back and, finally, the value of absorbed energy is constant after the separation of composite plate and impactor. The difference between the absorbed energy and the impact energy is the elastic energy that is converted again in the kinetic energy transferred to the impactor. The FEM model was able to accurately reproduce all these stages in absorbed energy evolution.

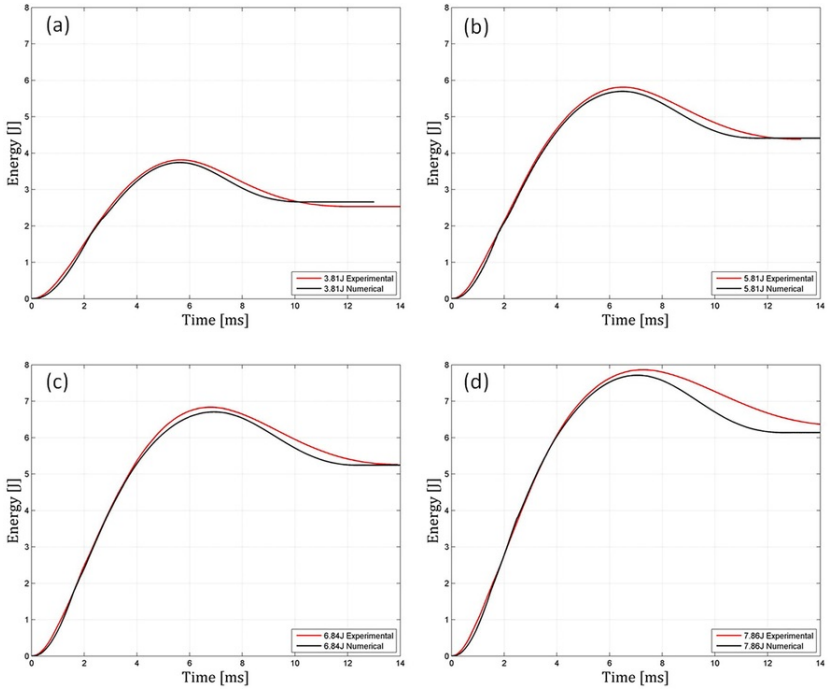

Fig. 5 Evolution of absorbed energy for different impact energies. Impactor nose with ϕ12.7 mm. (a) Eimp = 3.81 J. (b) Eimp = 5.81 J. (c) Eimp = 6.84 J. (d) Eimp = 7.86 J.

Figs. 4 and 5 only show the results with the impactor nose of ϕ12.7 mm, the results with the impactor nose of ϕ20 mm were similar. The evolution of absorbed energy with impact energy is represented in Fig. 6 for both impactors. Again, a reasonable agreement was obtained when the experimental and numerical result were compared. An almost linear increment of absorbed energy with impact energy was observed. When comparing different impactor noses at the same impact energy, the absorbed energy is almost identical. The main difference is that the impactor with higher diameter can be subjected to a higher impact energy before penetration.

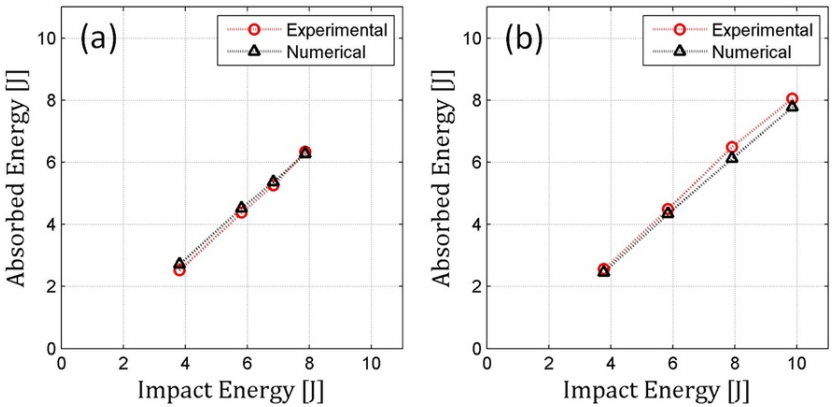

Fig. 6 Absorbed energy as a function of impact energy. Numerical predictions and experimental data for (a) impactor nose with ϕ12.7 mm and (b) impactor nose with ϕ20 mm.

Not only global variables as contact force or absorbed energy were reproduced by FEM numerical model but also failure mode. When traditional composites are subjected to an impact energy lower than the penetration energy, the main failure modes are delamination and matrix cracking. However, damage modes in natural based composites are quite different, the main failure mode in the impacted specimens was fibre failure as was reported by Huber et al.

[14] on Cordenka fibres based composites. C-Scan ultrasonic inspection was used to analyse internal damage but no delamination was found in any impacted specimen. Fig. 7 shows that failure mode consisted on the formation of four petals due to two perpendicular cracks in a cross shape, this failure mode is similar to that reported in Ref. [14]. The FEM model was able to accurately reproduce the formation of the two perpendicular cracks and the petals, the cracks also grew along the fibres directions and the cracks length was similar to those found in experimental tests.

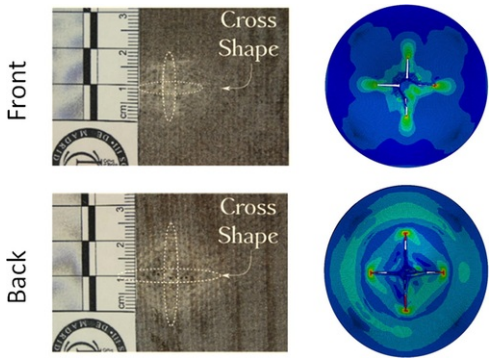

Fig. 7 Cross shape failure mode with an impact energy of 7.86 J and impactor nose of ϕ12.7 mm. Experimental specimens and FEM model.

Since no delamination was observed in the impacted specimens, experimental values of damaged area were defined using the permanent deflection. The damaged area was defined as the points with a permanent deflection higher than 1 mm. This area was assumed elliptical, so that two perpendicular axes were measured to calculate damaged area. The permanent deflection in the impacted face was measured by means of a laser extensometer MEL M27L/50. The laser was attached to an automatic positioning system to measure not only the maximum permanent deflection, but also the deflection along a path in the specimen. The damaged area in FEM results was also assumed elliptical. The lengths of the two cracks were used as the axes of the elliptical damaged area.

The evolution of the damaged area with impact energy for both impactor noses is shown in Fig. 8. For both impactor noses damaged area increases with impact energy and the slope of the curves also increases with impact energy. The maximum value of damaged area was found when the specimens were impacted with the impactor of larger diameter.

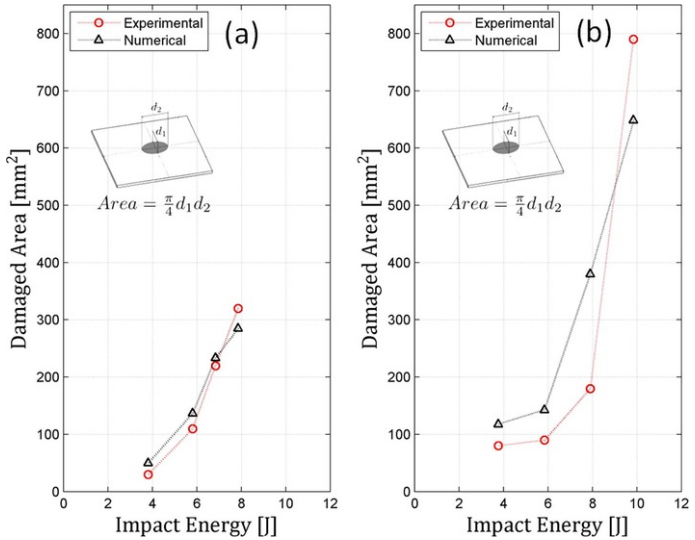

Fig. 8 Damaged area as a function of impact energy. Numerical predictions and experimental data for (a) impactor nose with ϕ12.7 mm and (b) impactor nose with ϕ20 mm.

Numerical results are in a reasonable agreement with experimental data, FEM model was able to reproduce the trends observed experimentally. However, numerical results overestimated damaged area for lower impact

energies and underestimated it for impact energy near to penetration energy. These differences can be neglected in the case of the impactor nose with ϕ12.7 mm, but they are significant in the case of ϕ20 mm. These differences can be attributed to the greater extension of damage with the impactor nose with ϕ20 mm and the influence of boundary conditions. The composite plate was clamped between two steel rings leaving a free circular surface with a diameter of 55 mm. For sake of simplicity, only the free surface of the composite plate was modelled, considering that the external surface was perfectly clamped. This simplified hypothesis has been proved to be valid to analyse contact forces, absorbed energy and failure modes for both impactor noses but the estimation of damaged area is more sensible to boundary conditions.

5 Conclusions

A constitutive model considering the influence of strain rate on the mechanical behaviour of biocomposites was implemented to analyse the impact behaviour of flax/PLA composites. The constitutive model considers non-linear mechanical behaviour as a function of strain-rate and a failure criterion based on maximum strains to delete damaged elements.

The model is validated through the simulation of low-velocity impacts. Numerical predictions were in agreement with experimental results in terms of force history, evolution of absorbed energy and failure modes for all the impact energies analysed and both impactor noses. Significant differences were found in the prediction of damage area with the impactor nose of ϕ20 mm at higher impact energies. These discrepancies can be attributed to the influence of boundary conditions when the extension of damage is near to the plate edges.

The main contributions of the model are based on the differences between conventional composites and natural fibres based composites. Conventional composites can be considered linear-elastic up to failure and the influence of strain-rate is usually neglected. However, experimental tests conducted by different authors have shown the need to consider plastic behaviour and the influence of strain rate to predict the dynamic behaviour of biocomposites. The present work is the first attempt to include viscoplastic behaviour in a predictive FEM model. The accuracy of the results can open a promising line of research that can lead to a new generation of FEM models for natural fibres based composites.

Acknowledgments

Authors gratefully acknowledges the support of Spanish Ministry of Economy under the project DPI2013-43994-R.

References

[1] F.P. La Mantia and M. Morreale, Green composites: a brief review, *Compos Part A Appl Sci Manuf* **42**, 2011, 579–588.

[2] H. Essabir, R. Boujmal, M.O. Bensalah, D. Rodrigue, R. Bouhfid and A. el Kacem Qaiss, Mechanical and thermal properties of hybrid composites: oil-palm fiber/clay reinforced high density polyethylene, *Mech Mater* **98**, 2016, 36–43.

[3] A.N. Netravali and S. Chabba, Composites get greener, *Mater Today* **6** (4), 2003, 22–29.

[4] Y.S. Song, J.T. Lee, D.S. Ji, M.W. Kim, S.H. Lee and J.R. Youn, Viscoelastic and thermal behavior of woven hemp fiber reinforced poly(lactic acid) composites, *Compos Part B* **43**, 2012, 856–860.

[5] B. Bax and J. Müssig, Impact and tensile properties of PLA/Cordenka and PLA/flax composites, *Compos Sci Technol* **68** (7), 2008, 1601–1607.

[6] T. Gurunathan, S. Mohanty and S.K. Nayak, A review of the recent developments in biocomposites based on natural fibres and their application perspectives, *Compos Part A Appl Sci Manuf* 2015, 1–25.

[7] G. Koronis, A. Silva and M. Fontul, Green composites: a review of adequate materials for automotive applications, *Compos Part B Eng* **44** (1), 2013, 120–127.

[8] R. Jayakumar, D. Menon, K. Manzoor, S.V. Nair and H. Tamura, Biomedical applications of chitin and chitosan based nanomaterials—a short review, *Carbohydr Polym* **82** (2), 2010, 227–232.

[9] C. Santiuste, S. Sanchez-Saez and E. Barbero, Residual flexural strength after low-velocity impact in glass/polyester composite beams, *Compos Struct* **92**, 2010, 25–30.

[10] V. Antonucci, F. Caputo, P. Ferraro, A. Langella, V. Lopresto, V. Pagliarulo, et al., Low velocity impact response of carbon fiber laminates fabricated by pulsed infusión: a review of damage investigation and semi-empirical models validation, *Prog Aerosp Sci* **81**, 2015, 26–40.

[11] I. Ivañez, C. Santiuste and S. Sanchez-Saez, FEM analysis of dynamic flexural behaviour of composite sandwich beams with foam core, *Compos Struct* **92** (9), 2010, 2285–2291.

[12] W. Tan, B.G. Falzon, L.N.S. Chiu and M. Price, Predicting low velocity impact damage and compression-after-impact (CAI) behaviour of composite laminates, *Compos Part A Appl Sci Manuf* **7**, 2015, 212–226.

[13] C. Santiuste, S. Sanchez-Saez and E. Barbero, A comparison of progressive-failure criteria in the prediction of the dynamic bending failure of composite laminated beams, *Compos Struct* **92** (10), 2010, 2406–2414.

[14] T. Huber, S. Bickerton, J. Müssig, S. Pang and M.P. Staiger, Flexural and impact properties of all-cellulose composite laminates, *Compos Sci Technol* **88**, 2013, 92–98.

[15] H.N. Dhakal, M. Skrifvars, A. Adekunle and Z.Y. Zhang, Falling weight impact response of jute/methacrylated soybean oil bio-composites under low velocity impact loading, *Compos Sci Technol* **92**, 2014, 134–141.

[16] A. Rubio-López, J. Artero-Guerrero, J. Pernas-Sánchez and C. Santiuste, Compression after impact of flax/PLA biodegradable composites, *Polym Test* **59**, 2017, 127–135.

[17] A. Rubio-López, A. Olmedo and C. Santiuste, Modelling impact behavior of allcellulose composite plates, *Compos Struct* **122**, 2015, 139–143.

[18] F. Wang, X. Li, J. Zhang, L. Li and L.M. Keer, Micromechanical modelling of the progressive failure in unidirectional composites reinforced with bamboo fibres, *Mech Mater* **94**, 2016, 180–192.

[19] Y. Pan and Z. Zhong, A micromechanical model for the mechanical degradation of natural fiber reinforced composites induced by moisture absorption, *Mech Mater* **85**, 2015, 7–15.

[20] I.J. Beyerlein and C.M. Landis, Shear-lag model for failure simulations of unidirectional fiber composites including matrix stiffness, *Mech Mater* **31** (5), 1999, 331–350.

[21] J.A. Nairn, On the use of shear-lag methods for analysis of stress transfer in unidirectional composites, *Mech Mater* **26** (2), 1997, 63–80.

[22] A. Rubio-López, T. Hoang and C. Santiuste, Constitutive model to predict the viscoplastic behaviour of natural fibres based composites, *Compos Struct* **155**, 2016, 8–18.

[23] C. Poilâne, Z.E. Cherif, F. Richard, A. Vivet, B.B. Doudou and J. Chen, Polymer reinforced by flax fibres as a viscoelastoplastic material, *Compos Struct* **112** (1), 2014, 100–112.

[24] A. Rubio-López, A. Olmedo, A. Díaz-Álvarez and C. Santiuste, Manufacture of compression moulded PLA based biocomposites: a parametric study, *Compos Struct* **131**, 2015, 995–1000.

[25] S. Ochi, Mechanical properties of kenaf fibers and kenaf/PLA composites, *Mech Mater* **40** (4), 2008, 446–452.

[26] O.H. Yeoh, Some forms of the strain energy function for rubber, *Rubber Chem Technol* **66** (5), 1993, 754–771.